

Weak Gravitational Lensing around Field Galaxies in HST Survey Images

R. E. Griffiths, S. Casertano, M. Im & K. U. Ratnatunga

Bloomberg Center for Physics and Astronomy, Johns Hopkins University, Homewood Campus, Baltimore, MD 21218, USA

ABSTRACT

Using data from the HST Medium Deep Survey, a long-term Key Project, together with generically similar archived data, we have discovered evidence for weak gravitational ‘shear’ of background field galaxies ($I = 22 - 26$) in the vicinity of isolated, foreground galaxies ($I = 15 - 22$), especially those of early type. The statistical lensing is demonstrated by the slight preferential orientation of the major axes of the background galaxies in directions at right angles to the lines joining them to the foreground ones. The detected shear is at the level of $\delta\phi = 2.5^\circ \pm 1.2^\circ$ averaged over the background galaxies at about ~ 10 half-light radii from 400 foreground ellipticals, corresponding to a polarization of about 0.04. A positive but less significant result is also reported for foreground spirals. This result excludes the de Vaucouleurs model for the mass distribution of ellipticals, but is consistent with elliptical galaxies having total $M/L \sim 100$ and extensive dark halos.

Key words: gravitational lensing, dark matter

1 INTRODUCTION

The first attempt to detect the weak gravitational shear of background galaxies by isolated foreground field galaxies was made by Tyson et al (1984) who catalogued field galaxies between $m_J = 19 - 21.5$ (where the J magnitude is approximately equal to Johnson B) and searched for polarisation in nearby field galaxies with magnitudes between $m_J = 22.5 - 23.5$. These authors inferred a 2σ upper limit on the average mass of the brighter foreground galaxies at $1.7 \times 10^{11} M_\odot$, with a corresponding limit on the rotational velocity of 170 km s^{-1} for a mass envelope extending to beyond 50 kpc (this limit was subsequently revised by Kovner and Milgrom (1987) to about 330 km s^{-1}). Tyson et al used photographic plates in moderate seeing ($2'' - 3''$), and the results from these early studies were negative or inconclusive. Using CCD data with good atmospheric seeing, however, Brainerd et al (1996) have claimed that polarisation has indeed been detected, for background field galaxies between $23 < r < 24$ mag and within about 35 arcs of foreground galaxies between $19 < r < 23$ mag.

The Wide Field and Planetary Camera 2 (WFPC2 – Trauger et al 1994) on the Hubble Space Telescope produces (nearly) diffraction-limited images which are ideal for these studies, since ellipticities and position angles can be measured routinely to $I = 24$ in summed exposures of about 30 mins. on each of 2 – 3 HST earth-orbits. The field of view is small (a total WFC area of 5.0 sq. arc mins.) so that data are needed from large numbers of fields in order to accumulate a large enough number of galaxies to form useful statistics. The HST Medium Deep Survey using WFPC2 commenced in January 1994 and has since accumulated a sufficient number of fields that we have been able to initiate a search for

these effects. Furthermore, a primary WFPC2 survey consisting of 28 contiguous fields was performed by Groth et al (1994) in April 1994 and these data have been obtained from the HST archive.

2 OBSERVATIONS

The MDS uses data taken with WFPC2 operating in parallel mode, using the F606W filter for the V-band and F814W for the I-band (Griffiths et al 1994a, 1994b). We have excluded fields dominated by stellar images. The MDS sample is uniformly distributed over the sky with $|b| \geq 20$ deg, with the detection limit of each field ranging over $I \simeq 23 \sim 25$ and $V \simeq 24 \sim 25.5$ (see Neuschaefer et al. 1996). For the purposes of the present study, the WFPC2 MDS dataset has been combined with the strip survey of Groth et al. This 42 arc min long strip consists of 28 contiguous WFPC2 fields which extend along the direction of galactic latitude, with the survey center at $b = +60^\circ.25$ and $l = 96^\circ.35$. The total area is about 120 square arc minutes when we exclude the 0.6 sq arc min overlap between adjacent fields. The twenty-eight fields were observed for 2800s (4x700s) in F606W and 4400s (4x1100s) in F814W.

The calibrated data from the MDS and Groth strip were run through the automated object finder and classifier developed for the MDS project (Ratnatunga et al 1994). We have corrected the geometric distortion near the boundary of CCDs using the solution of Holtzman et al (1995) in order to avoid spurious detection of signal (See Section 5). For each object detected, the observed image is fitted with simple model profiles (point source, $r^{1/4}$ profile or ‘bulge’, and exponential profile or ‘disk’) using a 2-dimensional technique of maximum likelihood estimation or MLE (Ratnatunga et

al 1994). MLE object classification is then based on the luminosity profile. Structural parameters such as axis ratio, size (r_{hl} , angular half light radius) and total magnitude result from the best model fit, which also gives the position angle of the major axis of each galaxy. Near the completeness level of the survey, the noise from the MLE fits is three times less than the corresponding noise resulting from the use of image moments measured using standard data analysis packages such as FOCAS (Jarvis and Tyson 1981).

We detected 475+/-25 objects in each of the Groth strip fields, and a similar number in MDS fields of comparable depth. After removal of stars and duplicate (confused) objects we thus produced a catalog of about 28,000 objects, of which about 10,000 galaxies are brighter than the completeness magnitude of $I=25$. Full details of the catalog and statistical analyses of the results therefrom are described in other publications by the MDS group.

The foreground ‘lens’ galaxy candidates are objects classified as bulge, disk or (unclassified) galaxies with $15 < I < 22$ in the object catalogs (1600 total, of which about 400 are E/S0 galaxies). The high resolution HST data have made it possible to separate these potential lensing populations, in a way which cannot be done using ground-based data. The background ‘source’ galaxy candidates are objects classified as bulge, disk, or (unclassified) galaxies with $22 < I < 26$ (14,000 total).

3 GALAXY MASS DISTRIBUTION MODELS

The galaxy mass density profile is modeled as a softened isothermal sphere (see Krauss & White 1992; Kochanek 1996), the shape of which is determined by the core radius (r_c), velocity dispersion (σ), and truncation radius r_t , beyond which the mass density becomes zero. For E/S0 galaxies, the core radius is taken to be $r_c = 0.05r_{hl}$ (Kochanek 1996), and for spirals $r_c = 0.5r_{hl}$ (Binney & Tremaine 1987), where the half light radius r_{hl} is a function of the luminosity following the relation described in Im et al. (1995a). The velocity dispersion scales as a function of the luminosity, following the Faber-Jackson relation (for E/S0s) or the Tully-Fisher relation (for Spirals; $\sigma = V_c/\sqrt{2}$, here V_c is circular velocity), and we adopt parameters for the relation those used by Kochanek (1996) and Brainerd et al. (1996). The truncation radius r_t is treated as a free parameter which is assumed to scale with r_{hl} . The truncation radius determines the extent of the dark halo in galaxies, and is thus an important parameter for the measurement of the total mass to light ratio.

For elliptical galaxies, we also modeled the mass profile using the de Vaucouleurs profile, with a constant mass to light (M/L) ratio, since the light profile of ellipticals follow this model (de Vaucouleurs 1948). For the M/L ratio of this model, we assume the mass to near infrared light ratio of $(M/L_I)/(M_{\odot}/L_{\odot,I}) = 20h$, which roughly corresponds to an upper limit of the M/L ratio at the core of elliptical galaxies (e.g, de Zeeuw & Franx 1991). For the redshift distribution of galaxies, we use the functional form described by Efsthathiou (1995), controlled by one input parameter, the median redshift z_{med} . The redshift distribution of the foreground galaxies is rather well defined by spectroscopic surveys (Lilly et al 1995) and by our own data. For our elliptical galaxies, we obtained $z_{med} = 0.6$, estimating redshifts

photometrically (Im et al. 1996). Lilly et al. (1995) found $z_{med} \simeq 0.5$ for galaxies with $I < 22$, and we will adopt this value for spiral galaxies. The value of z_{med} for the background galaxies ($22 < I < 26$) is unknown but very likely $z_{med} < 3$ (Guhathakurta et al. 1990). We will set z_{med} of the background galaxies equal to 2, and explore the effect of smaller values. For the observed axis ratio distribution of background galaxies, we use the axis ratio distribution of disk galaxies in Im et al. (1995b).

4 DETECTION OF WEAK SHEAR

The gravitational shear of background galaxy images causes them to be preferentially oriented in the direction perpendicular to the radius vector to the foreground galaxy. The ‘‘relative position angle’’ ϕ is the position angle of the major axis of the background galaxy, measured counter-clockwise from the radius vector to the foreground galaxy. When we fitted galaxy models to the images, we implicitly assumed that galaxies are symmetric with respect to a 180° rotation, and ϕ is therefore defined between 0° and 180° . All values of ϕ are in principle equivalent, on the assumption that the foreground and background galaxies are physically unrelated. Gravitational shear can in principle be detected as a deviation of the distribution of ϕ from uniformity. This deviation depends on the strength of the gravitational shearing effect, measured by the ‘‘image polarization’’ p , which is the induced ellipticity in an intrinsically circular image. In the limit of weak shear that we consider, the polarization p equals the difference between the tangential and the radial stretch due to the lensing. In practice, the gravitational shear will lead to a small bias towards values of ϕ around 90° .

Different measures have been suggested for the deviation of ϕ from a uniform distribution. The most obvious method is to consider the ‘‘reduced position angle’’ ϕ_{red} in the range ($0^\circ, 90^\circ$), obtained by taking either ϕ or $180^\circ - \phi$ as required; this is equivalent to merging together clockwise and counter-clockwise deviations. The average value of the reduced position angle is a measure of the non-uniformity of the distribution induced by the gravitational shear. A second possibility is to express the distribution as a Fourier series; for the range ($0^\circ, 180^\circ$), only $\cos(m\phi)$ terms are required. The effect of the gravitational shear will manifest itself primarily as a negative $\cos(2\phi)$ term.

A third possibility is to estimate directly the polarization as $p \approx -(1 - r^2)/(1 + r^2)\cos(2\phi)$, where r is the measured image axis ratio; this is closely related to the parameter χ used by Brainerd et al (1995). Use of this third indicator is made difficult by the fact that only 30% of the (usually faint) source galaxies have reliable measurements of the axis ratio. Since the results are comparable to those of the Fourier decomposition, this method is not considered further here.

4.1 Results

Figure 1 shows the average value of the reduced relative position angle, as a function of θ/r_{hl} . The average is larger than 45° because gravitational shear makes the tangential alignment ($\phi_{red} \sim 90^\circ$) more likely than the radial alignment ($\phi_{red} \sim 0^\circ$). The results of the model calculations are

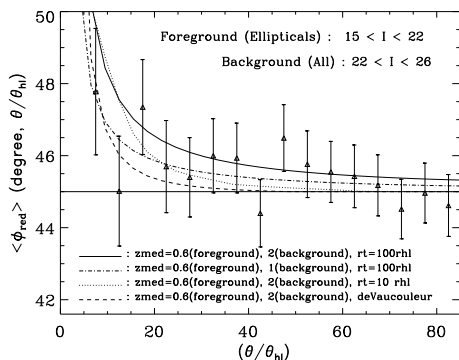


Fig. 1(a). The mean reduced position angle $\langle \phi_{red} \rangle$ of source galaxies binned as a function of radial distance from the foreground ellipticals, where the radial distances are normalized by the r_{hl} of the ellipticals

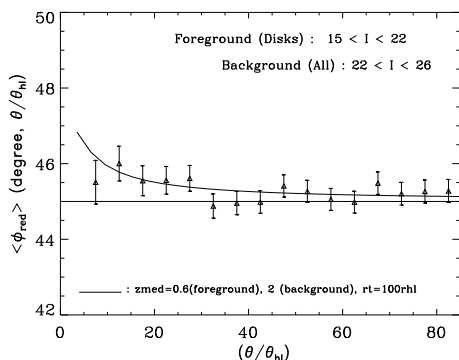


Fig. 1(b). The mean reduced position angle $\langle \phi_{red} \rangle$ of source galaxies binned as a function of radial distance from the foreground spirals, where the radial distances are normalized by the r_{hl} of the spirals

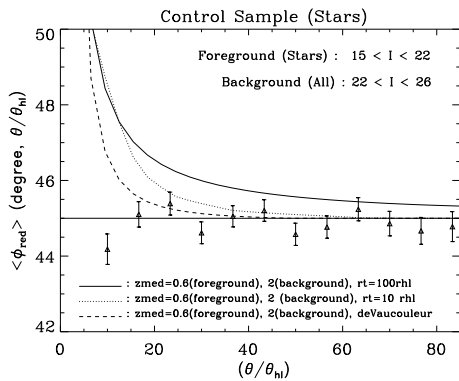


Fig. 1(c). The mean reduced position angle $\langle \phi_{red} \rangle$ of “source” galaxies binned as a function of radial distance from the foreground stars, where the stars have been taken as a control sample ($\theta_{hl} = 0''.5$ is used for this figure)

compared to the detected weak lensing signal in Fig. 1. The observed signal for ellipticals stays strong at least out to about 50 half-light radii, and is well matched by a model with $r_t = 100 r_{hl}$. The de Vaucouleur model and the isothermal sphere model with $r_t = 10 r_{hl}$ both fail to match the observed signal, suggesting that the M/L of ellipticals is not constant and that the mean truncation radius is much larger

than 10 half-light radii ($\gtrsim 30 kpc$ for a L_* galaxy). The effect of changing z_{med} for the redshift distribution is such that a stronger signal is obtained using a high z_{med} . But reducing z_{med} does not reconcile the data with the de Vaucouleur model. Since early-type galaxies are known to cluster more than spirals (Neuschaefer et al. 1996 have shown this for the same data set as that used here), several tests were made to ensure that the lensing signal was not produced by clusters rather than the ellipticals themselves. The fields each contain several E/S0s and the tests involved shifting the assumed centers of the potentials to points which might likely be close to the possible ‘cluster’ centers. All such tests produced null results for the lensing signal.

For the rest of the foreground galaxies (mostly spirals), the observed signal is considerably weaker (Fig.1-b). This is an expected trend because the late-type galaxies have less mass and shallower profile near the center than ellipticals. But again we see that the observed signal is well matched by the isothermal sphere model with $r_t = 100 r_{hl}$. No signal is observed in a control sample with stars as “foreground” objects (Fig.1-c; See also section 5).

It is interesting to note that the observed signal shows $r_t \gg 10 r_{hl}$. If $r_t \simeq 100 r_{hl}$, then the M/L of the lensing galaxies is about a few hundred. This value is comparable to the M/L of clusters of galaxies, suggesting that 1) the mass of clusters can be explained by the sum of the masses of cluster members; and that 2) $\Omega_{matter} \sim 0.1$. A full comparison between the models and the data, with a full discussion of the image polarisation, will be presented by Kneib et al (in preparation).

4.2 Fourier-series decomposition

The results of a Fourier-series decomposition of the distribution of relative position angle ϕ for the full sample are shown in Fig. 2 as a function of θ/r_{hl} , where θ is the apparent angular separation between source and lens centers and r_{hl} is the half-light radius of the lens. For this analysis, subsample of galaxies more than 150 pixels from the edge of CCDs is used in order to avoid false signal due to the geometric distortion at the boundary of the CCD (See section 5). Fourier terms are normalized as a fraction of the $m = 0$ term; formally, the m^{th} term is given by $A_m = 2\langle \cos(m\phi_i) \rangle$, where the index i spans all the sources considered. Only the $m = 2$ term shows a significant deviation from zero, as predicted by the gravitational lensing effect. The relationship between polarization and A_2 depends on the axis ratio distribution of source galaxies; for an average ellipticity of 0.56, as observed in our data for galaxies in the range $22 < I < 26$ mag, we obtain $p \approx 0.26A_2$.

Different subdivisions of the sample, by properties of the lens and of the background sources, show the polarization signal to different degrees. In Fig. 2 we show the amplitude of the A_2 component separately for ellipticals and spirals, as well as for all lenses. The signal is clearly stronger for elliptical galaxies than for spirals. (In fact, the signal for faint lenses and for spirals is not statistically significant.) This is in line with the predictions of the isothermal sphere models, shown as thin lines in each plot.

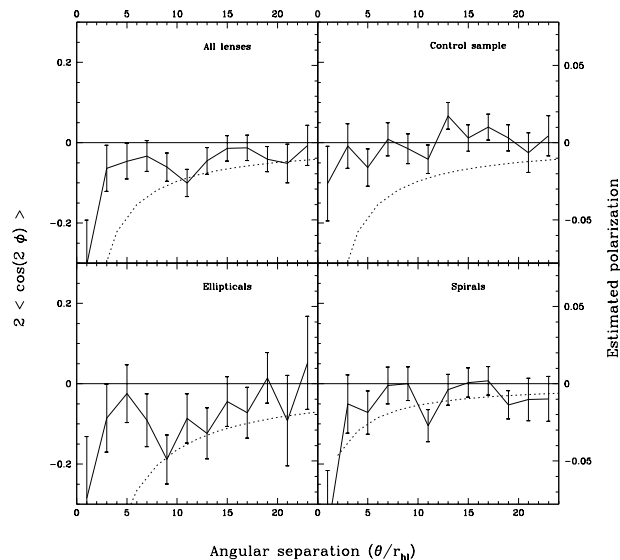


Fig. 2. Weak lensing signal as measured by a Fourier-series decomposition method. The model curve corresponds to the solid line in fig. 1a

5 TESTS FOR SYSTEMATIC ERRORS

The effect of gravitational shear is a subtle one, and therefore special care must be exercised to identify and prevent a number of small problems that could give a false signal, or mask and/or weaken an existing signal. One such problem is the possibility of faint pieces of the lens galaxy itself, such as pieces of spiral arms at large distance from the center, masquerading as background galaxies. This is potentially a problem at separations of 1–2 r_{hl} (it may be the origin of some of the signal seen at small separation in the whole sample and the spirals in Fig. 2), but it is extremely unlikely to be significant at 10 r_{hl} , where a strong signal can still be seen. Also, it would affect preferentially the spiral galaxies, and the observed signal at large radial distances is much stronger for ellipticals. The observed signal could potentially be affected by other galaxies on the lines of sight to the background sources. We have examined those galaxies within separations of 15 r_{hl} of the ellipticals, where we find that there are fainter ellipticals (by up to 1 mag.) in less than 10% of cases; we conclude that the effect on the observed signal is negligible.

Another potential problem is the geometric distortion of the WFPC2 field of view. For systems near the edges of the field, this induces a small artificial rotation of the galaxy images that could result in a spurious alignment. We have tested this in several ways. First, a subsample using only systems more than 150 pixels from the edges shows the same qualitative distortion as the full sample. Second, a test has been carried out in which “foreground” and “background” galaxies close in pixel position, *but in different fields*, have been associated; any geometric distortion effect would have been visible in this sample, but a null signal was detected (control sample in Fig. 2). A null signal was also detected

when using stars as centers (Figure 1c). Finally, the geometric distortion has been modeled and corrected using the solution of Holtzman et al (1995); this allows lenses and sources from different camera heads to be considered as an ensemble, and has been used in the average angle calculation (Fig. 1). However, we find that the geometric correction does not influence the signal significantly.

6 SUMMARY AND CONCLUSIONS

We have discovered evidence for weak galaxy-galaxy shear in data from the HST Medium Deep Survey and archived HST survey data. The weak lensing signal extends out to 50 half light radii from the foreground galaxies, and results in a mean position angle of about 47.5 degrees at around 10 half-light radii for ellipticals, and 46 degrees for spirals (compared with a null of 45 degs.). This result is consistent with a simple lensing model for the foreground galaxies which employs a softened singular isothermal sphere with $r_t = 100r_{hl}$, or at least $r_t \gg 10r_{hl}$, and $\sigma_c^* = 220\text{km/sec}$ for the central velocity dispersion of L^* ellipticals and $V_c^* = 220\text{km/sec}$ for the circular velocity of L^* spirals. However, a constant M/L de Vaucouleurs model for the mass profiles fails to fit the observed lensing signals for ellipticals and is excluded.

ACKNOWLEDGMENTS

This paper is based on observations with the NASA/ESA Hubble Space Telescope, obtained at the Space Telescope Science Institute, which is operated by the Association of Universities for Research in Astronomy, Inc., under NASA contract NAS5-26555. The Medium Deep Survey is funded by STScI grant GO2684 *et seq.* We gratefully acknowledge help with the MDS pipeline processing and analysis by Lyman Neuschaefer and Eric Ostrander, and many helpful discussions with R.S.Ellis, J.A.Tyson, J.-P. Kneib and T. Ebbels.

7 REFERENCES

- Binney, J. J. & Tremaine, S. D., 1987, in “Galactic Dynamics”, Princeton: Princeton University Press
- Brainerd, T. G., Blandford, R. D. & Smail, I., 1996, ApJ, in press
- Efstathiou G., 1995, MNRAS, 272, L25
- Griffiths, R. E. et al 1994a, ApJ, 437, 67
- Griffiths, R. E., et al., 1994b, ApJ, 435, L19
- Groth, E. J., Kristian, J. A., Lynds, R., O’Neil, E. J., Balsano, R., Rhodes, J., 1994, BAAS, 26, 1403
- Guhathakurta P., Tyson J. A., & Majewski, S. R., 1990, ApJ, 357, L9
- Holtzman, J., et al., 1995, PASP, 107, 156
- Im, M., Casertano, S., Griffiths, R. E., Ratnatunga, K. U., & Tyson, A. J., 1995a, ApJ, 441, 494
- Im, M., Ratnatunga, K. U., Griffiths, R. E., & S. Casertano, 1995b, ApJ, 445, L15
- Im, M., Griffiths, R. E., Ratnatunga, K. U. & Sarajedini, V. L. 1996, ApJ, 461, L79
- Jarvis, J. F., & Tyson, J. A., 1981, AJ, 86, 476
- Kochanek, C. S., 1996, ApJ, submitted
- Kovner, I. & Milgrom, M., 1987, ApJ 321, L113
- Krauss, L. M. & White, M. 1992, ApJ, 394, 385
- Lilly, S., et al., 1995, ApJ, 455, 108

Neuschaefter, L. W., Im, M., Ratnatunga, K. U., Griffiths, R. E.
& Casertano, S., 1996, ApJ, in press
Ratnatunga, K. U., Griffiths, R. E., Casertano, S., Neuschaefter,
L.W., & Wyckoff, E. W., 1994, AJ, 108, 2362
Trauger, J. T., et al., 1994, ApJ 435, L3
Tyson, J. A., Valdes, F., Jarvis, J. F., Mills, A. P., 1984, 281, L59
de Vaucouleurs, 1948, Ann.d'Astrophys., 11, 247
de Zeeuw, T., & Franx, M., 1991, ARAA, 29, 239